

## June–September mean temperature variability in the eastern Qinghai-Tibet Plateau over the past 225 years based on high quality tree-ring records

Xinyue Li <sup>a,b</sup>, Linlin Gao <sup>a,b,\*</sup>, Baolong Ma <sup>a,b</sup>, Kai Wang <sup>a,b</sup>, Yang Deng <sup>a,b</sup>

<sup>a</sup> Key Laboratory of Western China's Environmental Systems with the Ministry of Education (MOE), College of Earth and Environmental Sciences, Lanzhou University, Lanzhou 730000, China

<sup>b</sup> Gansu Liancheng Forest Ecosystem Field Observation and Research Station, Lanzhou 730333, China

### ARTICLE INFO

Editor: H. Falcon-Lang.

**Keywords:**

Tree-ring  
Reconstruction  
Mean temperature  
Eastern Qinghai-Tibet Plateau  
Northern Hemisphere  
Volcanic eruptions  
PDO  
AMO

### ABSTRACT

Being one of the most high-resolution climate proxies, tree-rings have been extensively used in paleoclimate studies, and help forecast future global warming and patterns of climate change. However, most climate reconstructions based on tree-ring data explain less than 50 % of the variance observed in meteorological station records, and high-quality chronologies are essential for a reliable assessment of climate change. Here, we present a new June–September mean temperature reconstruction over the past 225 years (1796–2020 CE) using *Abies faxoniana* tree-ring width data from the eastern Qinghai-Tibet Plateau, which explains 67.4 % of the instrumental temperature variations during 1960–2020 CE ( $r = 0.82$ ,  $p < 0.001$ ). This reconstruction shows significant ( $p < 0.01$ ) spatial representativeness for June–September temperature variations in the eastern Qinghai-Tibet Plateau and allows identification of significant ( $p < 0.05$ ) cycles at 2–4-, 54-, 79-, and 128-year periodicities. Three obvious cold periods in 1810s–1820s, 1910s–1930s, and 1960s–1980s were likely related to low solar activity and frequent volcanic eruptions, negative phases of Atlantic Multidecadal Oscillation and Pacific Decadal Oscillation, and enhanced anthropogenic aerosol-induced radiation dimming, respectively. Consistency with nearby temperature reconstructions and divergence with the Northern Hemisphere temperature variations suggest that more regional and high-quality tree-ring-based climate research should be conducted to advance our knowledge of climate variability.

### 1. Introduction

Anthropogenic global warming exerts profound influences on water and energy cycles, ecosystems, socioeconomic development, and human well-being (IPCC, 2021). The Qinghai-Tibet Plateau is recognized as a climate-sensitive and ecologically vulnerable region and is also regarded as the world's largest "Water Tower" (Immerzeel et al., 2010). Recent warming in the Qinghai-Tibet Plateau has occurred at twice the rate of the global average during 1961–2020 CE (Chen et al., 2015; You et al., 2015; Zhou et al., 2024), thereby impacting the cryosphere, hydrological resources, and ecosystem stability, as well as threatening socioeconomic sustainability. However, the short and scarce meteorological records in the Qinghai-Tibet Plateau and its surrounding areas limit the accurate assessment of current warming (Fan et al., 2010) and hinder our understanding of the long-term characteristics and patterns of climate variability (Zhu et al., 2011).

Tree rings, as one of the most important high-resolution climate proxies, have been extensively used in paleoclimate reconstructions globally (IPCC, 2021; Yuan et al., 2024), focusing on temperature (Esper et al., 2024; Bräuning and Mantwill, 2004), precipitation (Rodríguez-Catón et al., 2024), streamflow (Chen et al., 2023; Shi et al., 2024; Gao et al., 2021), and drought indices (Cook et al., 2010; Park Williams et al., 2013), among other related climate variables. Correlation coefficients are generally used to quantify tree growth–climate relationships and identify the target climate proxy in dendroclimatology (Büntgen and Esper, 2024). However, for most published reconstructions, the statistical correlation coefficients between tree-ring chronologies and instrumental records are typically below 0.7, meaning that tree-ring data can explain less than 50 % of the variance in climatic proxies. Given that tree growth is influenced by both intrinsic and extrinsic factors (e.g., hormones, phenology, temperature, precipitation, solar irradiance, competition, and microenvironment), explaining ~50 % of

\* Corresponding author at: Key Laboratory of Western China's Environmental Systems with the Ministry of Education (MOE), College of Earth and Environmental Sciences, Lanzhou University, Lanzhou 730000, China.

E-mail address: [gaoll@lzu.edu.cn](mailto:gaoll@lzu.edu.cn) (L. Gao).

the variance is generally considered acceptable for reliable climate reconstructions (Shi et al., 2013; Fritts, 1976). Nevertheless, dendrochronologists have continuously sought to improve reconstruction quality by exploring new tree-ring datasets, statistical approaches, and proxies (Büntgen and Esper, 2024).

In the Qinghai-Tibet Plateau, numerous dendrochronological studies have been conducted since the 1970s (Zhuo et al., 1978; Shao and Fan, 1999; Zhang et al., 2003; Liu et al., 2009; Gou et al., 2010; Yang et al., 2021). However, most of these tree-ring width records have been interpreted as reflecting precipitation and drought indices (Gou et al., 2014; He et al., 2019; Liu et al., 2025; Xiao et al., 2018), whereas temperature reconstructions based on ring-width and density data have mainly been conducted in the southeastern Qinghai-Tibet Plateau (He et al., 2019; Duan et al., 2017; Li et al., 2023; Li et al., 2015b; Yu et al., 2012). Among these studies, *Abies faxoniana*, a dominant subalpine conifer in the eastern Qinghai-Tibet Plateau, has been widely used for temperature reconstructions and is generally considered sensitive to growing-season temperatures (Table 1). Previous studies have reported moderate to strong correlations between tree growth and temperature, although the explained variance ( $R^2$ ) varies considerably among sites and seasons, with only a few reconstructions achieving relatively high values (Xiao et al., 2015; Wu et al., 2025). Given the significant topographic variations and altitudinal gradients in the eastern Qinghai-Tibet Plateau, which lead to pronounced spatial heterogeneity in climate responses, robust regional temperature reconstructions based on high-quality tree-ring chronologies are essential for accurately assessing local climate variability and identifying potential driving mechanisms.

In this study, we present a new tree-ring width chronology based on *Abies faxoniana* trees in the eastern Qinghai-Tibet Plateau. Based on this chronology, we try to improve the explained variance of the temperature reconstruction and reduce uncertainty in climate change assessment. Then, we further explore the spatial-temporal variation characteristics and patterns of this reconstruction, and identify the potential driving mechanisms of regional climate change in the eastern Qinghai-Tibet Plateau. This high-quality tree-ring based climate reconstruction will help us to better understand the recent climate conditions against the past variations.

## 2. Data and methods

### 2.1. Study area

The tree-ring sampling sites are located on the Western Sichuan Plateau in the eastern margin of the Qinghai-Tibet Plateau (Fig. 1a).

**Table 1**  
Overview of *Abies faxoniana* based climate reconstructions on the eastern Qinghai-Tibet Plateau.

Publication	Species	Location	Targeted climate factors	Reconstruction period (CE)	$R^2$	Correlation period (CE)
Li et al. (2010a)	<i>Abies faxoniana</i>	30.88°N, 102.98°E, 3450 m	June–August Mean Temperature	1850–2008	0.288	1955–2008
Wang et al. (2013)	<i>Abies faxoniana</i>	32.93°N, 104.33°E, 3150 m	February–June Mean Temperature	1755–2006	0.327	1959–2006
Chen et al. (2014)	<i>Abies faxoniana</i>	34.12°N, 103.80°E, 3120–3200 m	February–July Mean Temperature	1650–2006	0.435	1972–2006
Li et al. (2014)	<i>Abies faxoniana</i>	33.05°–32.66°N, 103.39°–103.72°E, 3290–3430 m	Annual Mean Temperature	1701–2010	0.332	1952–2010
Xiao et al. (2015)	<i>Abies faxoniana</i>	32.27°–32.28°N, 100.82°–103.38°E, 3530–3680 m	July–August Mean Temperature	1686–2010	0.546	1965–2010
Li et al. (2015a)	<i>Abies faxoniana</i>	31.63°N, 102.96°E, 4150 m	Annual Mean Temperature	1824–2009	0.467	1955–2002
Li et al. (2023)	<i>Abies faxoniana</i>	31.52°N, 101.70°E, 3000 m	June–July Mean Temperature	1733–2010	0.362	1962–2010
Li et al. (2024)	<i>Abies faxoniana</i> and <i>Sabina saltuaria</i>	31.39° N, 102.89° E, 3555 m	June–November mean temperature	1605–2016	0.373	1961–2016
Wu et al. (2025)	<i>Abies faxoniana</i> and <i>Picea asperata</i>	32.10°–33°N, 103.40°–103.70°E, 3290–3600 m	Annual Mean Temperature	1800–2018	0.599	1962–2018

There are pronounced altitudinal gradients in this region, with elevations ranging from approximately 5000 m in the western highlands to about 2000 m in the eastern lowlands, resulting in a total elevation difference of around 3000 m. The climate conditions here are modulated by the Indian Summer Monsoon and the mid-latitude westerlies. Based on records from the Hongyuan meteorological station (1960–2020), the mean monthly maximum temperature is 10.33 °C, the mean monthly minimum temperature is −5.23 °C, and the mean annual temperature is 1.74 °C. The average annual cumulative precipitation is above 600 mm (Fig. 1c), reflecting the typical climatic conditions of the region over the past six decades. Subalpine coniferous forests are the dominant vegetation in this area, mainly composed of *Picea asperata* and *Abies faxoniana*. Common shrubs include *Rhododendron* and *Potentilla fruticosa*, while herbaceous species are mainly *Kobresia*, *Festuca ovina*, and various alpine forbs such as *Gentiana* and *Saussurea* (Shen et al., 2021).

### 2.2. Tree-ring data

104 cores from 56 trees were collected from two pure *Abies faxoniana* forests in the Mengbi Mountains (31.71°N–31.71°N, 102.30°E, 3880–4010 m) in the year of 2021 (Fig. 1). Sampling and processing adhered to standard dendrochronological protocols (Fritts, 1976). Healthy trees with large diameters at breast height (DBH) and without visible biotic damage and anthropogenic disturbance were selected. Using increment borers, 1–3 cores per tree were extracted at breast height. In the laboratory, the cores were mounted, air-dried, and sequentially sanded following International Tree-Ring Data Bank (ITRDB) standards. Cross-dating was implemented through visual and statistical methods to ensure temporal accuracy. Tree-ring width measurements were obtained using a Velmex (Velmex Inc., Bloomfield, NY, USA) measuring system with 0.001 mm precision. The measurement series were quality-checked using the COFECHA program (Holmes, 1983), with a series intercorrelation of 0.536 and a mean sensitivity of 0.162. Finally, 92 cores from 49 trees were retained for chronology development.

### 2.3. Climate data

Monthly climate records, including mean temperature (Tmean), maximum temperature (Tmax), minimum temperature (Tmin), and total precipitation (P) from 1960 to 2020 CE, were obtained from the Hongyuan Meteorological Station (32.48°N, 102.33°E; 3491.6 m a.s.l.), sourced from the China Meteorological Data Service Center (<http://dat.a.cma.cn/>). The Hongyuan station was selected due to its geographic

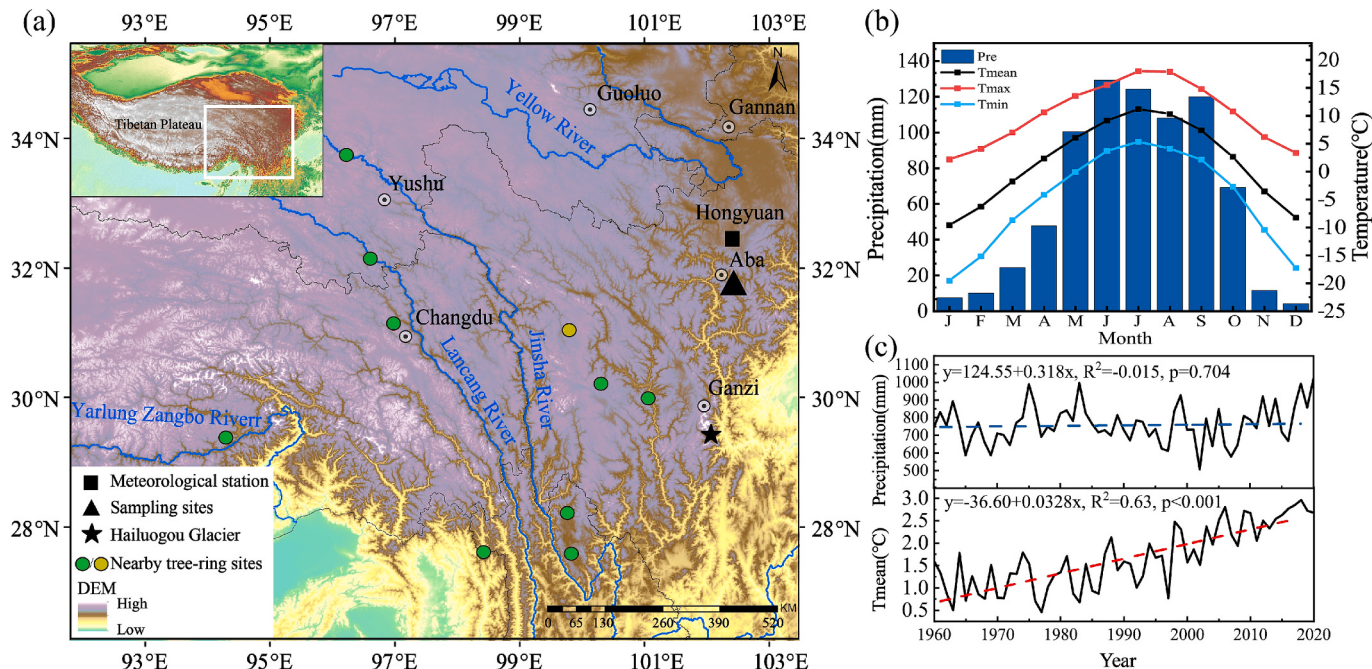


**Fig. 1.** (a) Map of the tree-ring sampling location (triangle) and the closest meteorological station (square, Hongyuan station). Nearby tree-ring records for comparisons shown in Fig. 5. The pentagram indicates the location of the Hailuogou Glacier. (b) Intra-annual variations of mean temperature, maximum temperature, minimum temperature, and precipitation recorded by the Hongyuan meteorological station. (c) Interannual variations in annual mean temperature and total precipitation from 1960 to 2020 CE.

proximity to the sampling sites (Fig. 1), which can represent the local climate conditions. The gridded monthly surface air temperature data from the CRU TS4.08 dataset ( $0.5^\circ \times 0.5^\circ$  resolution; Harris et al., 2020) were used to assess the spatial representativeness of the reconstruction. To explore the potential drivers of regional temperature variability, the sea surface temperature (SST) datasets, including HadSST4.0.0.0 ( $0.5^\circ \times 0.5^\circ$  resolution; Kennedy et al., 2019) and ERSSTv5 ( $2^\circ \times 2^\circ$  resolution; Huang et al., 2017), provided by the National Oceanic and Atmospheric Administration (NOAA), were used. Large-scale climate indices were obtained from the KNMI Climate Explorer (<http://climexp.knmi.nl>), including the Pacific Decadal Oscillation (PDO) index (Mann et al., 2009) and the Atlantic Multidecadal Oscillation (AMO) index (Mann et al., 2009). The Ice Core Volcanic Index (IVI) time series developed by Gao et al. (2008) were used to detect the role of volcanically forced temperature variations in the past.

#### 2.4. Methods

The Signal-Free method was applied in this study to remove non-climatic growth trends from the individual ring-width series and retain low-frequency climatic signals in the final chronology (Melvin and Briffa, 2008). The stabilized signal-free chronology was developed using the RCSsigFree software (<http://www.ldeo.columbia.edu/tree-ring-laboratory/resources/software>). The negative exponential function was used as the initial detrending curve. The quality of the chronology was evaluated using the inter-series correlation (Rbar), and the expressed population signal (EPS)  $> 0.85$  was used to determine the period of reliable signal representation (Wigley et al., 1984).

Pearson correlation analysis was used to identify the main climatic limiting factors for tree radial growth and the target reconstruction proxy. A linear regression model was employed to develop the reconstruction equation. The split-period calibration and verification tests were applied to assess the temporal stability and reliability of the model (Cook and Kairiukstis, 1990), using the statistics of Pearson correlation coefficient (r), coefficient of determination ( $R^2$ ), sign test (ST), reduction of error (RE), and coefficient of efficiency (CE). To assess extreme

climate events, years with values above (below) the mean by  $1.5\sigma$  were defined as extremely warm (cold) years, while periods with 11-year smoothed values remaining above (below) the mean for at least 11 consecutive years were defined as extremely warm (cold) phases.

To evaluate the spatial representativeness of the reconstruction, the spatial correlation analysis (Trouet and Van Oldenborgh, 2013) was conducted between the reconstructed temperature series and the gridded mean land surface temperature data using the KNMI Climate Explorer platform (<http://climexp.knmi.nl>). We also compared the reconstructed series with other adjacent dendroclimatic records and the Northern Hemisphere multiproxy temperature reconstruction series, to investigate the synchronization of local temperature variations with close regions and Northern Hemisphere. The Multi-Taper Method (MTM) spectral analysis (Mann and Lees, 1996) was employed to identify the dominant periodicities of climate variability embedded in the reconstruction. Composite analyses of sea surface temperature (SST) anomalies were performed to explore potential oceanic drivers of regional temperature variability using the NOAA PSL online tool (<http://psl.noaa.gov/cgi-bin/data/composites/printpage.pl>). Differences were computed with warm years minus cold years. Since ERSSTv5 data started from 1854 CE, the ten maximum and minimum values were selected from 1854 to 2020 in the high-pass-filtered reconstructed series. Superposed epoch analysis (SEA; Haurwitz and Brier, 1981) was used to analyze the influence of volcanic eruptions on regional temperatures using R scripts provided by Rao et al. (2019). The SEA was conducted over a 16-year window, including the year of the eruption, five preceding years, and ten subsequent years. A Monte Carlo resampling approach with 1000 iterations at the 95 % confidence level was used to evaluate the statistical significance of the volcanic signals.

## 3. Results

### 3.1. The tree-ring chronologies and proxy-target correlations

Tree cores from two *Abies faxoniana* sampling sites were combined to develop a composite chronology, as trees from the two sites exhibited

highly consistent variations in ring widths (Fig. 2a). The two independent tree-ring chronologies also showed significant correlations ( $r = 0.45$  for 1800–2021,  $p < 0.01$ ). The combined chronology from 1796 to 2020 was used for the reconstruction because the replication was sufficient and the EPS exceeded the threshold of 0.85 during this period (Fig. 2b).

Pearson correlations between the tree-ring chronology and meteorological records from the Hongyuan station showed strong positive correlations between tree radial growth and mean, minimum, and maximum temperatures for most months from the previous June to the current September (Fig. 2c–e). Nevertheless, the correlations with precipitation were weak and insignificant (Fig. 2f). These results indicate that temperature is the primary limiting climatic factor for *Abies faxoniana* tree growth in this high-mountain area. The highest correlation coefficient between tree-ring chronology and temperatures was found for the June–September mean temperature ( $r = 0.82$ ,  $p < 0.05$ ; Fig. 2c). The first-order difference correlation coefficient between reconstructed and observed June–September mean temperature is 0.53, which is lower than the original series, but it is still high and significant ( $p < 0.01$ ). This suggests that the tree-ring record might not capture some extremely high and low temperature years due to the adaptation and adjustment of trees to climate change.

### 3.2. June–September mean temperature reconstruction and spatial representativeness

Based on the above correlation analysis, the June–September mean temperature was defined as the target for reconstruction. We used a

linear regression model to develop the reconstruction as follows:

$$\text{Tmean} = 2.90 * W_t + 6.40 \quad (1)$$

$$(N = 61, R^2 = 67.35\%, r = 0.82, F = 121.68, p < 0.001)$$

In this equation, Tmean represents the reconstructed June–September mean temperature, and  $W_t$  indicates the tree-ring width index for the year of t. The reconstruction explains 67.35 % of the variance in the instrumental June–September mean temperature during 1960–2020 CE, providing the highest explained variance in this region so far (Table 1). The split-period calibration and verification statistics were used to examine the reliability of the reconstruction (Table 2). Both the reduction of error (RE) and coefficient of efficiency (CE) are positive, and the sign tests are significant at the 0.05 significance level. These metrics indicate that the reconstruction equation is statistically valid. Additionally, the reconstructed and observed June–September mean temperatures show overall consistency (Fig. 3b). All of the above evidence suggests that this reconstruction can reliably represent the actual June–September mean temperature variations in the eastern Qinghai-Tibet Plateau.

**Table 2**  
Calibration and verification statistics for the reconstruction model.

Period	$R^2$	Calibration		Verification		
		Period	r	ST	RE	CE
1960–1990	0.263	1991–2020	0.786	26+/4-	0.800	0.436
1991–2020	0.619	1960–1990	0.513	23+/8-	0.819	0.209
1960–2020	0.673					

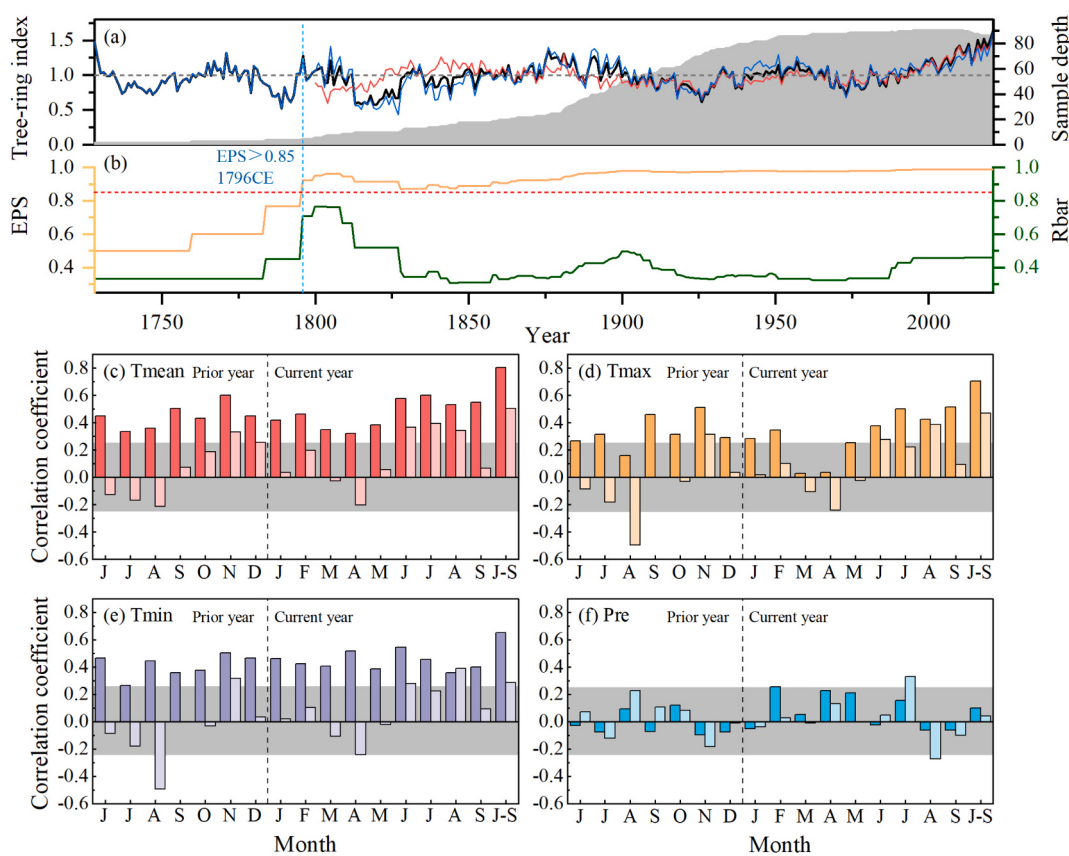


**Fig. 2.** (a) Tree-ring chronologies and the sample replications, with the black solid line and gray shaded area represent the combined chronology from two sites, while red and blue lines represent the independent tree-ring chronology from each site. (b) The expressed population signal (EPS) and inter-series correlation (Rbar) for the combined chronology. (c–f) Pearson's correlation coefficients between the combined tree-ring chronology and monthly mean temperature, maximum temperature, minimum temperature and monthly total precipitation for prior (June to December) and current year (January to September), as well as the seasonal combinations. The light bars in each plot indicate the first-difference correlation coefficients, and the gray shaded area suggests the significance level of 0.05. (For interpretation of the references to colour in this figure legend, the reader is referred to the web version of this article.)

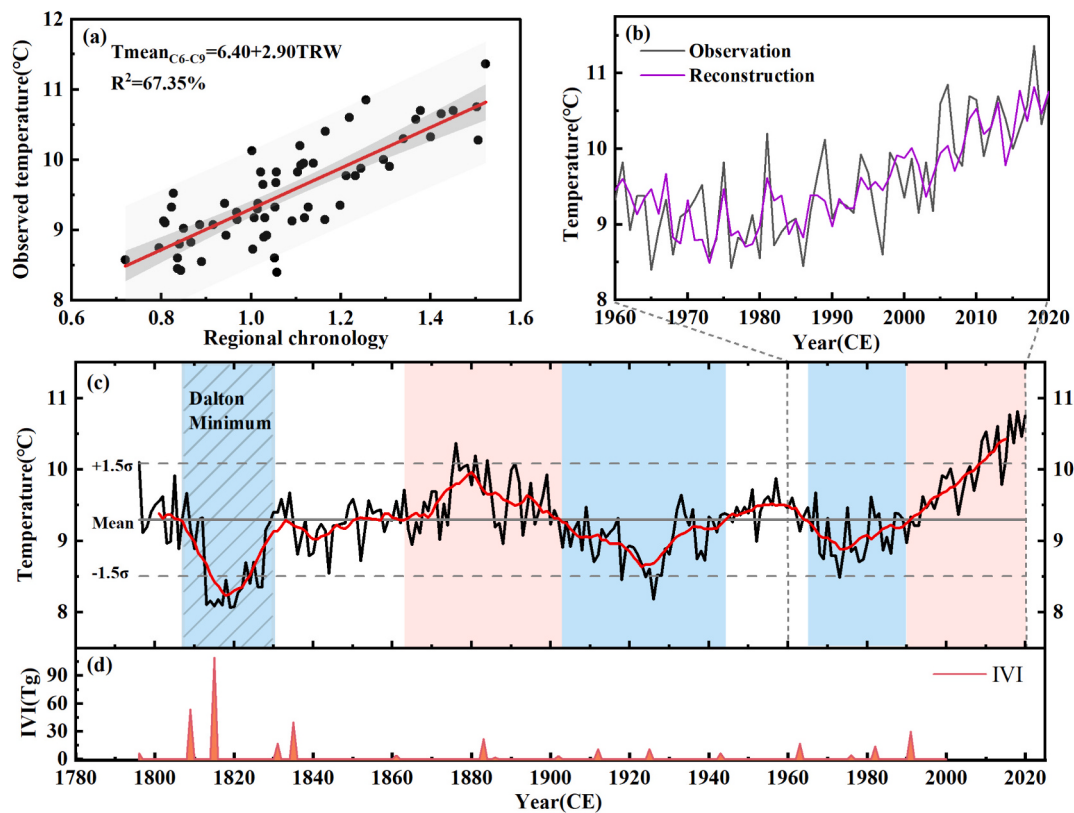


**Fig. 3.** Reconstructed June–September mean temperature for the period of 1796–2020 CE and comparisons between proxy and target data for the period of 1960–2020 (a–c). The red solid line in (c) represents the 11-year moving average of the reconstruction, while the blue and red shaded areas indicate the cold and warm periods, respectively. (d) The volcanic forcing index (IVI) from ice core records published by Gao et al. (2008), which was used here to evaluate the volcanically forced June–September temperature change in the eastern Qinghai-Tibet Plateau. (For interpretation of the references to colour in this figure legend, the reader is referred to the web version of this article.)

Tibet Plateau.

### 3.3. June–September mean temperature variations over the past 225 years

We reconstructed the June–September mean temperature for the period 1796–2020 CE in the eastern Qinghai-Tibet Plateau using the regression model (1). The reconstructed temperature variations over the past 225 years (Fig. 3c) show that the mean June–September temperature in this area is approximately 9.3 °C, with a standard deviation ( $\sigma$ ) of 0.52 °C. Temperature varied from the lowest of 8.07 °C in 1819 to the highest of 10.82 °C in 2018 during the past two centuries. When we defined extremely warm (cold) years as those with June–September mean temperatures exceeding the mean value plus (minus)  $1.5\sigma$ , sixteen extremely warm years were identified in 1796, 1876, 1881, 1884, 1891, 2009, 2010, 2011, 2012, 2013, 2015, 2016, 2017, 2018, 2019, and 2020, with 69 % of them occurring after 2000 CE. Similarly, seventeen extremely cold years were identified during 1813–1822, 1824, 1826, 1827, 1918, 1924, 1926, and 1973, with 76 % of them concentrated in 1810s–1820s during the Little Ice Age (1570–1900 CE; Matthews and Briffa, 2005; Yao et al., 1996). There were three obvious and prolonged (lasted for more than eleven consecutive years with smoothed temperatures below the mean) low temperature periods happened in 1807–1850, 1903–1944, and 1965–1990 CE, which were interrupted by two warm periods of 1863–1902 and 1954–1964. The warmest period of the past 225 years was from 1991 to 2020, which indicates that this reconstruction can successfully capture the recent anthropogenic warming in the eastern Qinghai-Tibet Plateau.

To further evaluate the reliability and spatial representativeness of the reconstruction, we compared it with gridded instrumental data.

Spatial correlation maps indicate that the reconstructed and instrumental June–September mean temperatures share similar spatial representativeness and strong correlations ( $r > 0.6, p < 0.01$ ) across the Qinghai-Tibet Plateau and northern China (Fig. 4a, b). Although the spatial correlations for the first-difference series decrease and narrow down to the eastern Qinghai-Tibet Plateau and Yellow River–Yangtze River basin (Fig. 4c, d), these results suggest that the reconstruction could successfully capture the temperature variability in the eastern Qinghai-Tibet Plateau and even extend over northern China at the low-frequency variability.

## 4. Discussion

### 4.1. June–September mean temperature variations in the eastern Qinghai-Tibet Plateau

The high correlations ( $r = 0.82, p < 0.01$ ) between the *Abies faxoniana* ring width chronology and instrumental June–September mean temperature indicate that higher June–September temperatures promote tree radial growth, making tree rings from the high mountains of the eastern Qinghai-Tibet Plateau a reliable proxy for temperature reconstruction. Compared with previous studies (Table 1), our reconstruction explains a substantially higher proportion of meteorological temperature variance ( $R^2 = 67.4 \%$ ), likely because *Abies faxoniana* is highly sensitive to growing-season temperature variations, and the sampling sites are located near the upper distribution limit of this species where tree growth is strongly constrained by temperature. The meteorological records from the Hongyuan station show that the average annual cumulative precipitation is above 600 mm in this area, and most of the precipitation falls in growing season (Fig. 1 b–c).

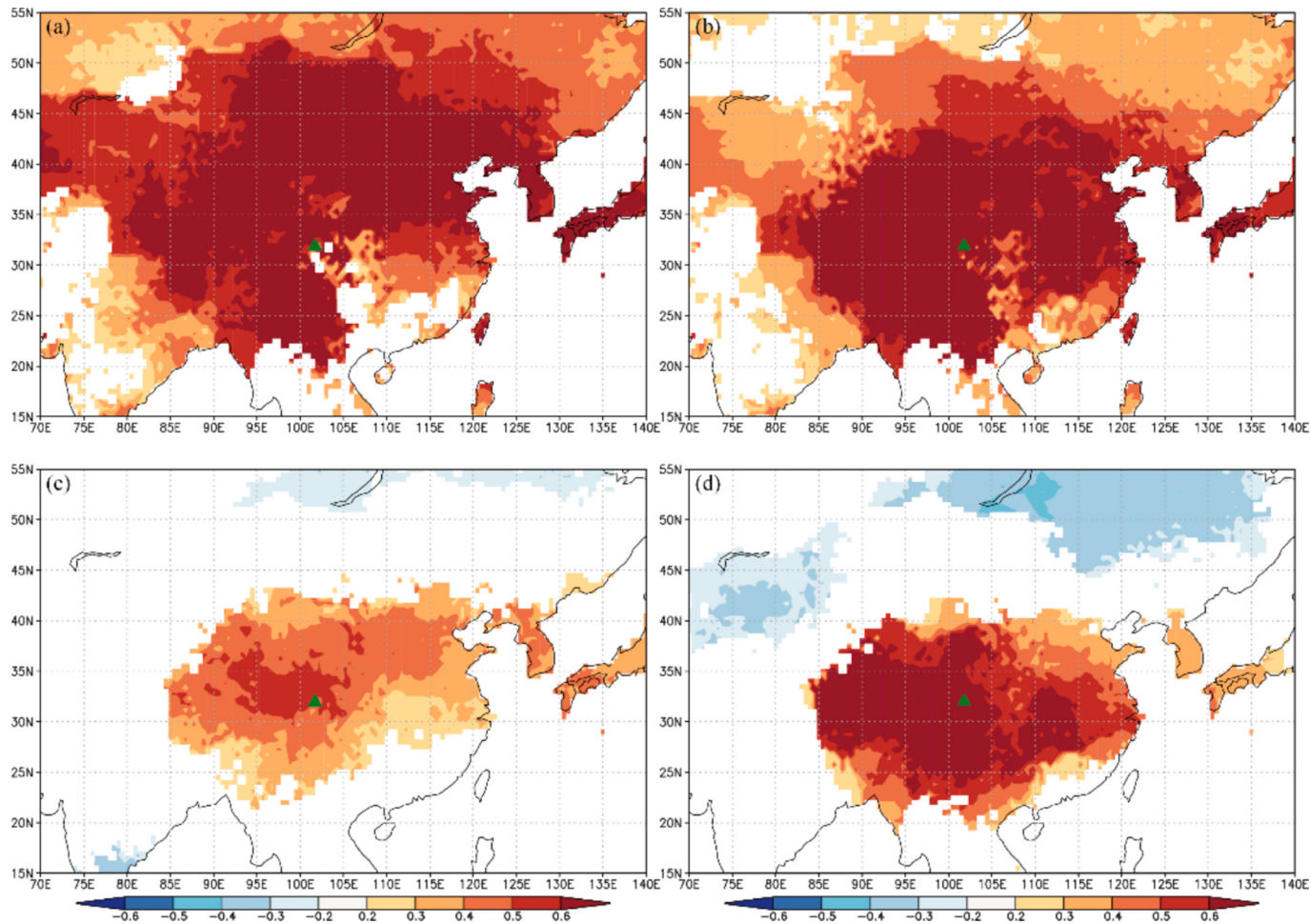


**Fig. 4.** Spatial correlations of the reconstructed (a) and instrumental (b) June–September mean temperatures with the gridded June–September mean temperature data from the CRU TS4.08 dataset for 1960–2020. (c) and (d) show the same thing but using the first-difference data. The green triangle represents the location of tree-ring record. (For interpretation of the references to colour in this figure legend, the reader is referred to the web version of this article.)

Therefore, the moisture conditions required for tree growth are sufficient, and then temperature acts as a primary limiting factor. Temperature impacts tree radial growth by regulating photosynthesis, cell division and expansion, as well as the duration of the growing season (Way and Oren, 2010; Cabon et al., 2020). Also, rising temperature in spring triggers soil thawing and initiates cambial activity of trees, which is especially important for trees growing at high elevations on the Qinghai-Tibet Plateau. Actually, *Abies faxoniana* is not the only tree species sensitive to temperature change in this area. *Picea balfouriana*, *Picea purpurea*, *Pinus densata*, *Abies fabri*, and *Sabina tibetica* have been extensively investigated and applied for temperature reconstructions but for different seasons and temperature related targets (Zhang et al., 2021; Yin et al., 2015; Liang et al., 2016; Li et al., 2021; Li and Li, 2017).

To evaluate the characteristics of June–September mean temperature variations in the eastern Qinghai-Tibet Plateau, we compared our reconstruction with two other temperature reconstructions from nearby regions (Deng et al., 2014; Wang et al., 2015), as well as with a hemispheric temperature reconstruction based on multi-proxy methods (Guillet et al., 2017). The results demonstrate high spatiotemporal synchrony of temperature variations in the eastern Qinghai-Tibet Plateau (Fig. 5a–c), which is consistent with the results of the spatial correlations between the reconstructed temperature and the gridded data (Fig. 4). The three temperature reconstructions show distinct cold periods in the 1810s–1820s, 1910s–1920s, and 1970s–1980s, while the cold period in the early part of the 19th century is even more pronounced in our reconstruction. The warm periods in 1930s–1950s and

after 1990s are common in these three reconstructions, but the relatively prolonged warm period in 1870s–1890s is more prominent in our reconstruction. These differences are likely related to the different data sources and tree species used for reconstructions. The terminus changes of the Hailuogou Glacier in the eastern Qinghai-Tibet Plateau also show high consistency with the tree-ring-based June–September temperature reconstructions, with rapid glacier retreat occurring during the warm periods of the 1930s–1960s and the 2000s, while the glacier remained relatively stable with a slow retreat rate during the cold period of the 1970s–1980s (Li et al., 2010b). To sum up, the June–September temperature variations in the eastern Qinghai-Tibet Plateau generally indicate similar patterns, suggesting three prominent cold phases (1810s–1820s, 1910s–1920s, and 1970s–1980s) and a dramatic warming trend after 1990s.

However, the June–September temperature variations in the eastern Qinghai-Tibet Plateau show noticeable difference at low frequencies with the Northern Hemisphere temperature over the past two centuries (Fig. 5d). The temperature increase started from the second half of the 19th century for the Northern Hemisphere, but some decadal warm and cold episodes were absent and insignificant in the Northern Hemisphere temperature reconstruction, which is also noted by Wang et al. (2015). Laepple et al. (2023) pointed out that climate variability at local scales often exceeds hemispheric averages, and climate models and large-scale reconstructions tend to underestimate the magnitude of multidecadal fluctuations observed in proxy records. Nevertheless, the prominent cold period in the 1810s–1840s and the relatively low-temperature period in

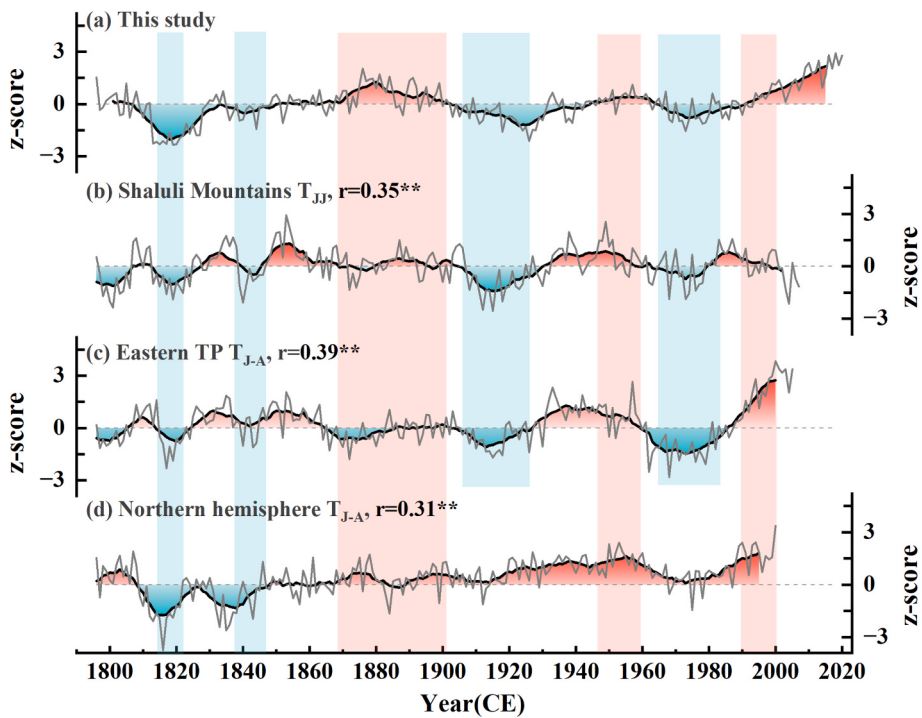


**Fig. 5.** Comparisons of temperature variations between the eastern Qinghai-Tibet Plateau and the Northern Hemisphere. The tree-ring-based temperature reconstructions in the eastern Qinghai-Tibet Plateau are from this study (a), Deng et al. (2014) (b), and Wang et al. (2015) (c). The Northern Hemisphere temperature reconstruction is from Guillet et al. (2017) (d), based on multiproxy records. The thin gray lines and bold black lines represent the annual values and 11-year moving averages, respectively, and all reconstructed series were standardized using the z-score method. The blue (orange) shaded rectangles highlight the synchronous cold (warm) temperature phases over the past two centuries. The values of  $r$  indicate the correlations between this reconstruction and others with original reconstructed series, and \*\* represents the significant level of  $p < 0.01$ . (For interpretation of the references to colour in this figure legend, the reader is referred to the web version of this article.)

the 1960s–1970s suggested by the Northern Hemisphere reconstruction are consistent with the temperature variations in the eastern Qinghai-Tibet Plateau (Fig. 5). Furthermore, the correlation between our June–September temperature reconstruction and the Northern Hemisphere reconstruction is 0.31 for 1796–2000 CE ( $p < 0.001$ ), suggesting partly synchronous temperature signals on a hemispheric scale. For instance, the prominent cold period in the early 19th century, considered one of the coldest phases of the Little Ice Age (LIA) and possibly of the entire Holocene (Büntgen et al., 2025; Essel et al., 2023), is likely a consequence of large-scale climate forcings, such as volcanic eruptions and ocean–atmosphere circulations (Yang et al., 2010; Liang et al., 2008).

#### 4.2. The possible driving mechanisms of June–September temperature variability

The period of the 1810s–1820s is identified as the coldest episode in the eastern Qinghai-Tibet Plateau from this June–September temperature reconstruction, which is also supported by other tree-ring, lake sediment, and glacier records (Zhu et al., 2016; Zhu et al., 2011; Hochreuther et al., 2015; Bräuning, 2006; Xu et al., 2012). Additionally, extreme cold events were identified in 1815, 1816, 1817, 1818, 1819, 1820, and 1821, following the 1815 volcanic eruption of Tambora, Indonesia. Then, we examined the volcanic impacts on June–September temperature in the eastern Qinghai-Tibet Plateau. There was a temporal cluster of large volcanic eruptions in 1809 (unidentified) and 1815 (Tambora, Indonesia) (Fig. 3d; Büntgen et al., 2025), which injected large amounts of sulfate aerosols into the stratosphere, reflecting solar radiation and forcing temperature decreases lasting from years to decades (Timmreck et al., 2021; Wagner and Zorita, 2005), resulting in the prominent cold period in the eastern Qinghai-Tibet Plateau and the Northern Hemisphere. The superposed epoch analysis (SEA) of the

June–September mean temperature response to volcanic eruptions with a Volcanic Explosivity Index (VEI)  $\geq 5$  indicates that significant cooling lasted for at least six years after the volcanic events (Fig. 6a), which supports that the extreme cold years of 1815–1821 in the eastern Qinghai-Tibet Plateau were a response to the 1815 Tambora eruption. In addition, the cold period of 1965–1990 may be linked to the eruptions of Agung volcano in 1963 and El Chichón in 1982 (Xu et al., 2024). These findings suggest that major volcanic eruptions have played an important role in influencing June–September temperature variability over the past two centuries in the eastern Qinghai-Tibet Plateau.

Several studies have reported the influences of volcanism on ENSO and its associated climatic impacts, for instance, an El Niño-like SST response during Northern Hemisphere extratropical eruption years (Dogar et al., 2023; Pausata et al., 2015). The MTM spectral analysis (Mann and Lees, 1996) of the reconstruction also suggests a possible linkage between ENSO and temperature variations in the eastern Qinghai-Tibet Plateau. There is a significant ( $p < 0.05$ ) 2–4-year cycle in the temperature reconstruction (Fig. 6b), which is consistent with the temporal scale of ENSO (Li et al., 2013; Bradley et al., 1987). The composite analysis of sea surface temperature anomalies between warm and cold years also reveals distinct El Niño-like SST anomalies (Fig. 6c). Furthermore, an independent tree-ring blue-intensity record of *Picea purpurea* from the eastern Qinghai-Tibet Plateau suggests ENSO as a key factor influencing summer maximum temperatures in this region (Qiao et al., 2024). ENSO might influence temperature variations in the eastern Qinghai-Tibet Plateau by modulating the intensity of the Western Pacific Subtropical High (WPSH) and the East Asian summer monsoon. During El Niño events, the Pacific–East Asian Teleconnection (P-EA) triggered by tropical Pacific warming weakens the East Asian summer monsoon and suppresses the transport of warm and moist airflows, leading to increased temperatures in the eastern Qinghai-Tibet Plateau (Wang et al., 2000; Zhang et al., 1996).

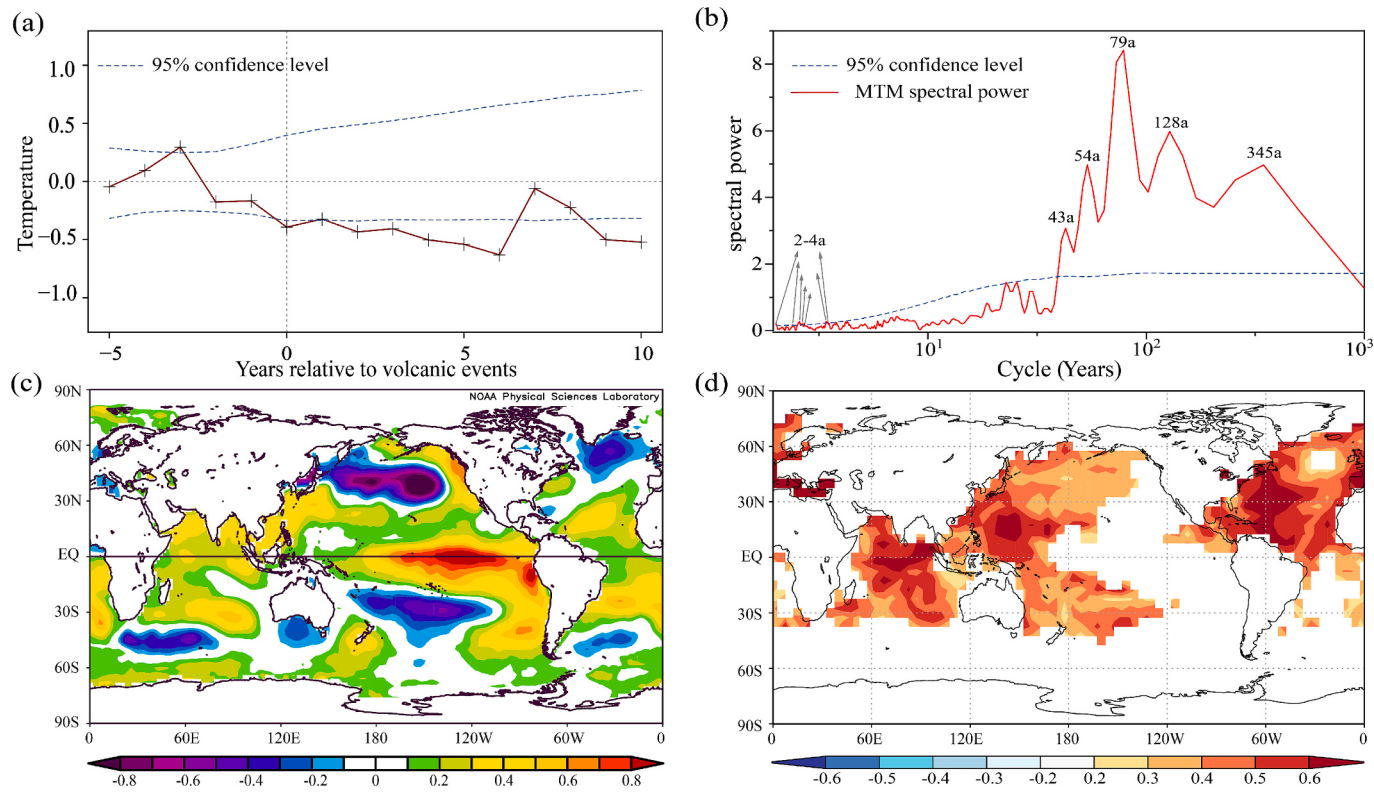


**Fig. 6.** (a) Superposed epoch analysis (SEA) of the June–September mean temperature response to volcanic eruptions, with the blue dashed lines representing the 95 % confidence intervals based on the Monte Carlo significance test. (b) Multi-taper spectral analysis (MTM) of the reconstructed June–September mean temperature in the eastern Qinghai-Tibet Plateau for 1796–2020 CE. The blue dashed line represents the 95 % confidence level, and the significant cycles are marked with peak values. (c) Composite analysis of sea surface temperature (SST) anomalies from November (previous year) to March (current year), based on ten extremely warm years and ten extremely cold years identified from this reconstruction. (d) Spatial correlation analysis between the reconstructed June–September mean temperature series and gridded global sea surface temperatures (HadSST4.0.0.0) at a  $0.5^\circ \times 0.5^\circ$  resolution for 1960–2020 CE. (For interpretation of the references to colour in this figure legend, the reader is referred to the web version of this article.)

The Atlantic Multidecadal Oscillation (AMO) and Pacific Decadal Oscillation (PDO) are also suggested as important large-scale climate modes that influence June–September mean temperature in the eastern Qinghai-Tibet Plateau over decadal timescales. Firstly, the significant ( $p < 0.05$ ) cycles of the temperature reconstruction are at 79-year, 54- and 43-year (Fig. 6b), which agree with the periodicity of AMO (65–70-year) and PDO (50–70-year) (Schlesinger and Ramankutty, 1994; MacDonald and Case, 2005). Then, the correlations between this June–September mean temperature reconstruction and the AMO ( $r = 0.42, p < 0.01$ ) and the PDO index ( $r = 0.47, p < 0.01$ ) from Mann et al. (2009) are strong and significant based on 11-year moving averages for the period 1796–2006. Moreover, the composite diagnostic analyses and spatial correlation analysis of the reconstructed June–September temperature with sea surface temperature (SST) show significant positive correlations between June–September temperature variability in the eastern Qinghai-Tibet Plateau and SST in the northern Atlantic and western Pacific (Fig. 6d). Wang et al. (2014) and Shi et al. (2019) found that the negative phase of the AMO, characterized by lower SST in the northern Atlantic, leads to lower temperatures in the eastern Qinghai-Tibet Plateau by regulating large-scale atmospheric circulation patterns. Similarly, the PDO influences temperature variability in this area by regulating the Asian monsoon system, with the negative phase of the PDO causing the western Pacific Subtropical High to weaken and shift eastward, thereby strengthening the East Asian summer monsoon and resulting in cooler and wetter conditions in the eastern Qinghai-Tibet Plateau. Actually, the cold phase of June–September temperature reflected by this reconstruction during 1910s–1930s corresponds to the negative phase of AMO and PDO in the early 20th century (Knight et al., 2006; Mantua and Hare, 2002).

Solar activity and radiation are also key factors influencing temperature variability in the eastern Qinghai-Tibet Plateau. The 128-year cycle indicated by our reconstruction might be associated with the Gleissberg cycle of solar activity (Peristykh and Damon, 2003), which has also been found in other temperature reconstructions in the eastern Qinghai-Tibet Plateau (Zhang et al., 2022; Wang et al., 2015; Yin et al., 2022). The variability in long-term solar activity may influence the climate system by modulating solar irradiance, cosmic ray-induced cloud formation, and heat transport within atmospheric and oceanic systems (Gray et al., 2010; Ogurtsov et al., 2002). Furthermore, the coldest period of June–September temperature (1810–1820s) over the past 225 years in the eastern Qinghai-Tibet Plateau happened in the Dalton Minimum (Hoyt and Schatten, 1993) (Fig. 3). A reconstruction of summer radiation and temperature over the Qinghai-Tibet Plateau by Jia et al. (2020) indicates that the post-1950 decrease in incoming shortwave radiation was primarily caused by anthropogenic aerosols. The rapid industrialization across Asia after the 1950s released substantial amounts of anthropogenic sulfate aerosols, which scattered incoming solar radiation and reduced surface temperatures. Therefore, this recent cold period during the 1960s–1980s might be linked to anthropogenic aerosol forcing.

## 5. Conclusions

In this study, we present a novel June–September mean temperature reconstruction in the eastern Qinghai-Tibet Plateau over the past 225 years (1796–2020 CE). This reconstruction is based on a high-quality tree-ring chronology developed from 92 tree-ring width series of *Abies faxoniana* trees from high-elevation mountains (3880–4010 m).

Significant positive correlations were found between the tree-ring chronology and mean, minimum, and maximum temperatures for most months of the growing season. In particular, the strongest correlation ( $r > 0.8$ ) was observed between the tree-ring chronology and the June–September mean temperature, which is significantly higher than most tree-ring-based climate reconstructions in this area. The spatial correlation maps also suggest the excellent agreement between proxies and climate targets, and reveal the strong spatial representativeness of June–September temperature reconstruction for the eastern Qinghai-Tibet Plateau. During the past two centuries, there were three obvious cold periods occurred in 1810s–1820s, 1910s–1930s, and 1960s–1980s, which were interrupted by two warm phases of 1863–1902 and 1945–1964. Rapid warming since the 1990s has resulted in the warmest temperatures in the past two decades for the eastern Qinghai-Tibet Plateau over the past two centuries. Notably, we found 76 % of the extremely cold years happened in the 1810s–1820s during the Little Ice Age era, while 69 % of the extremely hot years occurred after 2000 CE. Low solar irradiance during the Dalton Minimum (1790–1830) and an intense temporal cluster of large volcanic eruptions in 1809 and 1815 likely resulted in the coldest climate in the early 19th century. The MTM spectral analysis, composite diagnostic analyses, and spatial correlation analysis of the reconstruction with sea surface temperature (SST) suggest possible relationships between June–September temperature variability in the eastern Qinghai-Tibet Plateau and large-scale ocean–atmosphere circulations, such as ENSO, AMO, and PDO. Both the negative phases of the AMO and PDO in the early 20th century were indicated as important forcing factors for the June–September temperature decrease during 1910s–1930s by regulating the Asian monsoon system. When comparing our new reconstruction with the terminus changes of the Hailuogou Glacier, other temperature reconstructions in the eastern Qinghai-Tibet Plateau, and the Northern Hemisphere temperature, we found relatively synchronous temperature changes in the eastern Qinghai-Tibet Plateau, but noticeable differences at low frequencies compared with the Northern Hemisphere temperature. We conclude that high-resolution and high-quality paleoclimate reconstructions are needed for a robust understanding of regional climate change under anthropogenic global warming.

#### CRediT authorship contribution statement

**Xinyue Li:** Writing – original draft, Visualization, Methodology, Formal analysis, Data curation, Conceptualization. **Linlin Gao:** Writing – review & editing, Writing – original draft, Visualization, Validation, Supervision, Methodology, Funding acquisition, Formal analysis, Conceptualization. **Baolong Ma:** Writing – review & editing, Validation. **Kai Wang:** Writing – review & editing, Validation. **Yang Deng:** Writing – review & editing, Writing – original draft, Visualization, Validation, Supervision, Methodology, Formal analysis, Conceptualization.

#### Declaration of competing interest

The authors declare that they have no known competing financial interests or personal relationships that could have appeared to influence the work reported in this paper.

#### Acknowledgements

This work was supported by the National Natural Science Foundation of China (# 42571020; # 42430503). We thank the reviewers for their helpful comments and suggestions.

#### Data availability

All data used in this study are either freely available (<https://data.cma.cn/> and <https://climexp.knmi.nl>) or included in the online supplement.

#### References

- Bradley, R.S., Diaz, H.F., Kiladis, G.N., Eischeid, J.K., 1987. ENSO signal in continental temperature and precipitation records. *Nature* 327, 497–501. <https://doi.org/10.1038/327497a0>.
- Bräuning, A., 2006. Tree-ring evidence of ‘Little Ice Age’ glacier advances in southern Tibet. *Holocene* 16 (3), 369–380. <https://doi.org/10.1191/0959638306hl922rp>.
- Bräuning, A., Mantwill, B., 2004. Summer temperature and summer monsoon history on the Tibetan Plateau during the last 400 years recorded by tree rings. *Geophys. Res. Lett.* 31 (24), L24205. <https://doi.org/10.1029/2004GL020793>.
- Büntgen, U., Esper, J., 2024. Physiological meaning of bimodal tree growth-climate response patterns. *Int. J. Biometeorol.* 68 (9), 1897–1902. <https://doi.org/10.1007/s00484-024-02706-5>.
- Büntgen, U., Cosmo, N.D., Esper, J., Frachetti, M., Khalidi, L., Maelshagen, F., Rohland, E., Oppenheimer, C., 2025. Volcanoes, climate, and Society. *Annu. Rev. Earth Planet. Sci.* 54. <https://doi.org/10.1146/annurev-earth-032524-013254>.
- Cabon, A., Peters, R.L., Fonti, P., Martínez-Vilalta, J., De Cáceres, M., 2020. Temperature and water potential co-limit stem cambial activity along a steep elevational gradient. *New Phytol.* 226, 1325–1340. <https://doi.org/10.1111/nph.16456>.
- Chen, D.L., Xu, B.Q., Yao, T.D., Guo, Z.T., Cui, P., Chen, F.H., Zhang, R.H., Zhang, X.Z., Zhang, Y.L., Fan, J., Hou, Z.Q., Zhang, T.H., 2015. Assessment of past, present and future environmental changes on the Tibetan Plateau (in Chinese with English abstract). *Chin. Sci. Bull.* 60 (32), 3025–3035. <https://doi.org/10.1360/N972014-01370>.
- Chen, F., Yuan, Y.J., Wei, W.S., Yu, S.L., Shang, H.M., Zhang, T.W., Zhang, R.B., Wang, H.Q., Qin, L., 2014. Tree-ring based temperature reconstruction for the west Qinling Mountains (China): linkages to the High Asia, solar activity and Pacific-Atlantic Ocean. *Geochronometria* 41 (3), 234–244. <https://doi.org/10.2478/s13386-013-0159-9>.
- Chen, F., Man, W.M., Wang, S.J., Esper, J., Meko, D.M., Büntgen, U., Yuan, Y.J., Hadad, M., Hu, M., Zhao, X., Roig, F.A., Fang, O.Y., Chen, Y.P., Zhang, H.L., Shang, H.M., Yu, S.L., Luo, X.L., He, D.M., Chen, F.H., 2023. Southeast Asian ecological dependency on Tibetan Plateau streamflow over the last millennium. *Nat. Geosci.* 16, 1151–1158. <https://doi.org/10.1038/s41561-023-01320-1>.
- Cook, E.R., Kairiukstis, L.A., 1990. Methods of Dendrochronology: Applications in the Environmental Sciences. Springer, Netherlands, Dordrecht. <https://doi.org/10.1007/978-94-015-7879-0>.
- Cook, E.R., Anchukaitis, K.J., Buckley, B.M., D’Arrigo, R.D., Jacoby, G.C., Wright, W.E., 2010. Asian Monsoon failure and Megadrought during the last Millennium. *Science* 328 (5977), 486–489. <https://doi.org/10.1126/science.1185188>.
- Deng, Y., Gou, X.H., Gao, L.L., Yang, T., Yang, M.X., 2014. Early-summer temperature variations over the past 563 yr inferred from tree rings in the Shaluli Mountains, southeastern Tibet Plateau. *Quat. Res.* 81 (3), 513–519. <https://doi.org/10.1016/j.yqres.2013.08.002>.
- Dogar, M.M., Hermanson, L., Scaife, A.A., Visioni, D., Zhao, M., Hoteit, I., Graf, H.-F., Dogar, M.A., Almazroui, M., Fujiiwara, M., 2023. A Review of El Niño Southern Oscillation Linkage to strong Volcanic Eruptions and Post-Volcanic Winter Warming. *Earth Syst. Environ.* 7, 15–42. <https://doi.org/10.1007/s41748-022-00331-z>.
- Duan, J.P., Esper, J., Büntgen, U., Li, L., Xoplaki, E., Zhang, H., Wang, L.L., Fang, Y.J., Luterbacher, J., 2017. Weakening of annual temperature cycle over the Tibetan Plateau since the 1870s. *Nat. Commun.* 8, 14008. <https://doi.org/10.1038/ncomms14008>.
- Esper, J., Torbenson, M., Büntgen, U., 2024. 2023 summer warmth unparalleled over the past 2,000 years. *Nature* 631, 94–97. <https://doi.org/10.1038/s41586-024-07512-y>.
- Essel, H., Krusic, P.J., Esper, J., Wagner, S., Braconnor, P., Jungclaus, J., Muschitiello, F., Oppenheimer, C., Büntgen, U., 2023. A frequency-optimised temperature record for the Holocene. *Environ. Res. Lett.* 18, 114022. <https://doi.org/10.1088/1748-9326/ad0065>.
- Fan, Z.X., Bräuning, A., Tian, Q.H., Yang, B., Cao, K.F., 2010. Tree ring recorded May–August temperature variations since A.D. 1585 in the Gaoligong Mountains, southeastern Tibetan Plateau. *Palaeogeogr. Palaeoclimatol. Palaeoecol.* 296, 94–102. <https://doi.org/10.1016/j.palaeo.2010.06.017>.
- Fritts, H.C., 1976. Tree Rings and Climate. Academic Press, London.
- Gao, C., Robock, A., Ammann, C., 2008. Volcanic forcing of climate over the past 1500 years: An improved ice core-based index for climate models. *J. Geophys. Res.* 113 (D23). <https://doi.org/10.1029/2008JD010239>.
- Gao, L.L., Deng, Y., Yan, X.Y., Li, Q., Zhang, Y., Gou, X.H., 2021. The unusual recent streamflow declines in the Bailong River, north-Central China, from a multi-century perspective. *Quat. Sci. Rev.* 260, 106927. <https://doi.org/10.1016/j.quascirev.2021.106927>.
- Gou, X.H., Deng, Y., Chen, F.H., Yang, M.X., Fang, K.Y., Gao, L.L., Yang, T., Zhang, F., 2010. Tree ring based streamflow reconstruction for the Upper Yellow River over the past 1234 years. *Chin. Sci. Bull.* 55, 4179–4186. <https://doi.org/10.1007/s11434-010-4215-z>.
- Gou, X.H., Deng, Y., Chen, F.H., Yang, M.X., Gao, L.L., Nesje, A., Fang, K.Y., 2014. Precipitation variations and possible forcing factors on the Northeastern Tibetan Plateau during the last millennium. *Quat. Res.* 81 (3), 508–512. <https://doi.org/10.1016/j.yqres.2013.09.005>.
- Gray, L.J., Beer, J., Geller, M., Haigh, J.D., Lockwood, M., Matthes, K., Cubasch, U., Fleitmann, D., Harrison, G., Hood, L., Luterbacher, J., Meehl, G.A., Shindell, D., van Geel, B., White, W., 2010. Solar influences on climate. *Rev. Geophys.* 48 (4), RG4001. <https://doi.org/10.1029/2009RG000282>.
- Guillet, S., Corona, C., Stoffel, M., Sigl, M., Luterbacher, J., Wegmann, M., Tomé, C., Carrara, A., Frank, D., 2017. Climate response to the Samalas volcanic eruption in 1257 revealed by proxy records. *Nat. Geosci.* 10, 123–128. <https://doi.org/10.1038/NGEO2875>.

- Harris, I., Osborn, T.J., Jones, P., Lister, D., 2020. Version 4 of the CRU TS monthly high-resolution gridded multivariate climate dataset. *Sci Data* 7, 109. <https://doi.org/10.1038/s41597-020-0453-3>.
- Haurwitz, M.W., Brier, G.W., 1981. A critique of the superposed epoch analysis method: Its application to solar–weather relations. *Mon. Weather Rev.* 109 (10), 2074–2079. [https://doi.org/10.1175/1520-0493\(1981\)109<2074:ACOTSE>2.0.CO;2](https://doi.org/10.1175/1520-0493(1981)109<2074:ACOTSE>2.0.CO;2).
- He, M.H., Yang, B., Bräuning, A., Rossi, S., Ljungqvist, F.C., Shishov, V., Grießinger, J., Wang, J.L., Liu, J.J., Qin, C., 2019. Recent advances in dendroclimatology in China. *Earth Sci. Rev.* 194, 521–535. <https://doi.org/10.1016/j.earscirev.2019.02.012>.
- Hochreuther, P., Loibl, D., Wernicke, J., Zhu, H.F., Grießinger, J., Bräuning, A., 2015. Ages of major Little Ice Age glacier fluctuations on the southeast Tibetan Plateau derived from tree-ring-based moraine dating. *Palaeogeogr. Palaeoclimatol. Palaeoecol.* 422, 1–10. <https://doi.org/10.1016/j.palaeo.2015.01.002>.
- Holmes, R.L., 1983. Computer-assisted quality control in tree-ring dating and measurement. *Tree-Ring Bull.* 43, 69–78.
- Hooyt, D., Schatten, K., 1993. A discussion of plausible solar irradiance variations, 1700–1992. *J. Geophys. Res.* 98 (A11), 18895–18906. <https://doi.org/10.1029/93JA01944>.
- Huang, B., Thorne, P.W., Banzon, V.F., Boyer, T., Chepurin, G., Lawrimore, J.H., Menne, M.J., Smith, T.M., Vose, R.S., Zhang, H.-M., 2017. Extended reconstructed sea surface temperature, version 5 (ERSSTv5): upgrades, validations, and intercomparisons. *J. Clim.* 30, 8179–8205. <https://doi.org/10.1175/JCLI-D-16-0836.1>.
- Immerzeel, W.W., van Beek, L.P.H., Bierkens, M.F.P., 2010. Climate change will affect the Asian water towers. *Science* 328 (5984), 1382–1385. <https://doi.org/10.1126/science.1183188>.
- IPCC, 2021. Climate change 2021: the physical science basis. In: Masson-Delmotte, V., Zhai, P., Pirani, A., Connors, S.L., Péan, C., Chen, Y., Goldfarb, L., Gomis, M.I., Matthews, J.B.R., Berger, S., Huang, M., Yelekçi, O., Yu, R., Zhou, B., Lonnoy, E., Maycock, T.K., Waterfield, T., Leitzell, K., Caud, N. (Eds.), Contribution of Working Group I to the Sixth Assessment Report of the Intergovernmental Panel on Climate Change. Cambridge University Press, Cambridge, UK and New York, USA.
- Jia, A., Liang, S.L., Wang, D.W., Jiang, B.X., Zhang, X.L., 2020. Air pollution slows down surface warming over the Tibetan Plateau. *Atmos. Chem. Phys.* 20, 881–899. <https://doi.org/10.5194/acp-20-881-2020>.
- Kennedy, J.J., Rayner, N.A., Atkinson, C.P., Killick, R.E., 2019. An ensemble data set of sea surface temperature change from 1850: the Met Office Hadley Centre HadSST 4.0.0.0 data set. *J. Geophys. Res. Atmos.* 124, 7719–7741. <https://doi.org/10.1029/2018JD029867>.
- Knight, J.R., Folland, C.K., Scaife, A.A., 2006. Climate impacts of the Atlantic Multidecadal Oscillation. *Geophys. Res. Lett.* 33, L17706. <https://doi.org/10.1029/2006GL026242>.
- Laepple, T., Ziegler, E., Weitzel, N., Hébert, R., Ellerhoff, B., Schoch, P., Martrat, B., Bothe, O., Moreno-Chamarro, E., Chevalier, M., Herbert, A., Rehfeld, K., 2023. Regional but not global temperature variability underestimated by climate models at supradecadal timescales. *Nat. Geosci.* 16, 958–966. <https://doi.org/10.1038/s41561-023-01299-9>.
- Li, J.B., Xie, S.P., Cook, E.R., Morales, M.S., Christie, D.A., Johnson, N.C., Chen, F., D'Arrigo, R., Fowler, A.M., Gou, X.H., Fang, K.Y., 2013. El Niño modulations over the past seven centuries. *Nat. Clim. Chang.* 3, 822–826. <https://doi.org/10.1038/nclimate1936>.
- Li, J.J., Shao, X.M., Li, Y.Y., Qin, N.S., 2014. Annual temperature recorded in tree-ring from Songpan region (in Chinese with English abstract). *Chin. Sci. Bull.* 59 (15), 1446–1458. <https://doi.org/10.1360/972013-901>.
- Li, J.J., Jin, L.Y., Zheng, Z.Y., 2023. A 278-year Summer Minimum Temperature Reconstruction based on Tree-Ring Data in the Upper Reaches of Dadu River. *Forests* 14 (4), 832. <https://doi.org/10.3390/f14040832>.
- Li, J.X., Li, J.B., Li, T., Au, T.F., 2021. 351-year tree ring reconstruction of the Gongga Mountains winter minimum temperature and its relationship with the Atlantic Multidecadal Oscillation. *Clim. Chang.* 165 (3–4). <https://doi.org/10.1007/s10584-021-03075-3>.
- Li, T., Li, J.B., 2017. A 564-year annual minimum temperature reconstruction for the east central Tibetan Plateau from tree rings. *Glob. Planet. Chang.* 157, 165–173. <https://doi.org/10.1016/j.gloplacha.2017.08.018>.
- Li, T., Peng, J.F., Au, T.F., Li, J.R., Li, J.B., Zhang, Y., 2024. Dendroclimatological study of *Sabina saltuaria* and *Abies faxoniana* in the mixed forests of the Qionglai Mountains, eastern Tibetan Plateau. *J. For. Res.* 35, 20. <https://doi.org/10.1007/s11676-023-01664-9>.
- Li, Z.S., Liu, G.H., Zhang, Q.B., Hu, C.J., Luo, S.Z., Liu, X.L., He, F., 2010a. Tree ring reconstruction of summer temperature variations over the past 159 years in Wolong National Natural Reserve, western Sichuan, China (in Chinese with English abstract). *Chin. J. Plant Ecol.* 34 (6), 628–641. <https://doi.org/10.3773/j.issn.1005-264x.2010.06.002>.
- Li, Z.S., Liu, G.H., Gong, L., Wang, M., Wang, X.C., 2015a. Tree ring-based temperature reconstruction over the past 186 years for the Miyaluo Natural Reserve, western Sichuan Province of China. *Theor. Appl. Climatol.* 120 (3–4), 495–506. <https://doi.org/10.1007/s00704-014-1184-1>.
- Li, Z.S., Liu, G.H., Wu, X., Wang, X.C., 2015b. Tree-ring-based temperature reconstruction for the Wolong Natural Reserve, western Sichuan Plateau of China. *Int. J. Climatol.* 35, 3296–3307. <https://doi.org/10.1002/joc.4207>.
- Li, Z.X., He, Y.Q., Yang, X.M., Theakstone, W.H., Jia, W.X., Pu, T., Liu, Q., He, X.Z., Song, B., Zhang, N.N., Wang, S.J., Du, J.K., 2010b. Changes of the Hailiugou glacier, Mt. Gongga, China, against the background of climate change during the Holocene. *Quat. Int.* 218 (1–2), 166–175. <https://doi.org/10.1016/j.quaint.2009.09.005>.
- Liang, E.Y., Shao, X.M., Qin, N.S., 2008. Tree-ring based summer temperature reconstruction for the source region of the Yangtze River on the Tibetan Plateau. *Glob. Planet. Chang.* 61 (3–4), 313–320. <https://doi.org/10.1016/j.gloplacha.2007.10.008>.
- Liang, H.X., Lyu, L.X., Wahab, M., 2016. A 382-year reconstruction of August mean minimum temperature from tree-ring maximum latewood density on the southeastern Tibetan Plateau, China. *Dendrochronologia* 37, 1–8. <https://doi.org/10.1016/j.dendro.2015.11.001>.
- Liu, Y., An, Z.S., Linderholm, H.W., Chen, D.L., Song, H.M., Cai, Q.F., Sun, J.Y., Tian, H., 2009. Annual temperatures during the last 2485 years in the mid-eastern Tibetan Plateau inferred from tree rings. *Sci. China Ser. D-Earth Sci.* 52, 348–359. <https://doi.org/10.1007/s11430-009-0025-z>.
- Liu, Y., Song, H.M., An, Z.S., Qiang, L., Leavitt, S.W., Büntgen, U., Cai, Q.F., Liu, R.S., Fang, C.X., Sun, C.F., Treyte, K., Ren, M., Mo, L.D., Song, Y., Cai, W.J., Zhang, Q., Zhou, W.J., Bräuning, A., Grießinger, J., Chen, D.L., Linderholm, H.W., Sinha, A., Cheng, H., Wang, L., Zohner, C.M., 2025. Recent centennial drought on the Tibetan Plateau is outstanding within the past 3500 years. *Nat. Commun.* 16, 1311. <https://doi.org/10.1038/s41467-025-56687-z>.
- MacDonald, G.M., Case, R.A., 2005. Variations in the Pacific Decadal Oscillation over the past millennium. *Geophys. Res. Lett.* 32 (8), L08703. <https://doi.org/10.1029/2005GL022478>.
- Mann, M.E., Lees, J.M., 1996. Robust estimation of background noise and signal detection in climatic time series. *Clim. Chang.* 33, 409–445. <https://doi.org/10.1007/BF00142586>.
- Mann, M.E., Zhang, Z., Rutherford, S., Bradley, R.S., Hughes, M.K., Shindell, D., Ammann, C., Faluvegi, G., Ni, F., 2009. Global signatures and dynamical origins of the Little Ice Age and medieval climate Anomaly. *Science* 326, 1256–1260. <https://doi.org/10.1126/science.1177303>.
- Mantua, N.J., Hare, S.R., 2002. The Pacific Decadal Oscillation. *J. Oceanogr.* 58, 35–44. <https://doi.org/10.1023/A:1015820616384>.
- Matthews, J.A., Briffa, K.R., 2005. The ‘Little Ice Age’: Re-evaluation of an evolving concept. *Geogr. Ann. Ser. B* 87, 17–36. <https://doi.org/10.1111/j.0435-3676.2005.00242.x>.
- Melvin, T.M., Briffa, K.R., 2008. A “signal-free” approach to dendroclimatic standardisation. *Dendrochronologia* 26 (2), 71–86. <https://doi.org/10.1016/j.dendro.2007.12.001>.
- Ogurtsov, M.G., Nagovitsyn, Y.A., Kocharov, G.E., Jungner, H., 2002. Long-period cycles of the Sun’s activity recorded in direct solar data and proxies. *Sol. Phys.* 211, 371–394. <https://doi.org/10.1023/A:1022411209257>.
- Park Williams, A., Allen, C.D., Macalady, A.K., Griffin, D., Woodhouse, C.A., Meko, D.M., Swetnam, T.W., Rauscher, S.A., Seager, R., Grissino-Mayer, H.D., Dean, J.S., Cook, E.R., Gangodagamage, C., Cai, M., McDowell, N.G., 2013. Temperature as a potent driver of regional forest drought stress and tree mortality. *Nat. Clim. Chang.* 3, 292–297. <https://doi.org/10.1038/nclimate1693>.
- Pausata, F.S.R., Chafik, L., Caballero, R., Battisti, D.S., 2015. Impacts of high-latitude volcanic eruptions on ENSO and AMOC. *Proc. Natl. Acad. Sci. USA* 112 (45), 13784–13788. <https://doi.org/10.1073/pnas.1509153112>.
- Peristykh, A.N., Damon, P.E., 2003. Persistence of the Gleissberg 88-year solar cycle over the last ~12,000 years: evidence from cosmogenic isotopes. *J. Geophys. Res. Space Physics* 108 (A1). <https://doi.org/10.1029/2002JA009390>. SSH 1–1–SSH 1–15.
- Qiao, S.H., Deng, Y., Gao, L.L., Yuan, Y.Y., Huang, Q.L., Gou, X.H., 2024. Asymmetric impacts of El Niño–Southern Oscillation on summer temperature over the eastern Qinghai–Tibetan Plateau, as revealed by the blue intensity of *Picea purpurea*. *Glob. Planet. Chang.* 234, 104381. <https://doi.org/10.1016/j.gloplacha.2024.104381>.
- Rao, M.P., Cook, E.R., Cook, B.J., Anchukaitis, K.J., D'Arrigo, R.D., Krusic, P.J., 2019. A double bootstrap approach to Superposed Epoch Analysis to evaluate response uncertainty. *Dendrochronologia* 55, 119–124. <https://doi.org/10.1016/j.dendro.2019.05.001>.
- Rodríguez-Catón, M., Morales, M.S., Rao, M.P., Nixon, T., Vuille, M., Rivera, J.A., Oelkers, R., Christie, D.A., Varuolo-Clarke, A.M., Ferrero, M.E., Magney, T., Daux, V., Villalba, R., Andreu-Hayles, L., 2024. A 300-year tree-ring  $\delta^{18}\text{O}$ -based precipitation reconstruction for the South American Altiplano highlights decadal hydroclimate teleconnections. *Commun. Earth Environ.* 5, 269. <https://doi.org/10.1038/s43247-024-01385-9>.
- Schlesinger, M.E., Ramankutty, N., 1994. An oscillation in the global climate system of period 65–70 years. *Nature* 367, 723–726. <https://doi.org/10.1038/367723a0>.
- Shao, X.M., Fan, J.M., 1999. Past climate on West Sichuan Plateau as reconstructed from ring-widths of dragon spruce. *Quat. Sci.* 19 (1), 81–89 (in Chinese).
- Shen, C.M., Liu, K.B., Tang, L.Y., Overpeck, J., 2021. Modern pollen rain in the Tibetan Plateau. *Front. Earth Sci.* 9, 732441. <https://doi.org/10.3389/feart.2021.732441>.
- Shi, C.M., Sun, C., Wu, G.C., Wu, X.C., Chen, D.L., Masson-Delmotte, V., Li, J.P., Xue, J.Q., Li, Z.S., Ji, D.Y., Zhang, J., Fan, Z.X., Shen, M.G., Shu, L.F., Ciais, P., 2019. Summer temperature over the Tibetan Plateau modulated by Atlantic multidecadal variability. *J. Clim.* 32 (13), 4055–4067. <https://doi.org/10.1175/JCLI-D-17-0858.1>.
- Shi, J.F., Cook, E.R., Li, J.B., Lu, H.Y., 2013. Unprecedented January–July warming recorded in a 178-year tree-ring width chronology in the Dabie Mountains, southeastern China. *Palaeogeogr. Palaeoclimatol. Palaeoecol.* 381–382, 92–97. <https://doi.org/10.1016/j.palaeo.2013.04.018>.
- Shi, X.Y., Gao, L.L., Deng, Y., Zhang, Y.H., Zhang, X., Gou, X.H., 2024. A tree-ring based streamflow reconstruction for the Taohe River (Gannan Plateau, China) associated with the Asian-Pacific Oscillation since 1325 CE. *Catena* 241, 108027. <https://doi.org/10.1016/j.catena.2024.108027>.
- Timmreck, C., Toohey, M., Zanchettin, D., Brönnimann, S., Lundstad, E., Wilson, R., 2021. The unidentified eruption of 1809: a climatic cold case. *Clim. Past* 17, 1455–1482. <https://doi.org/10.5194/cp-17-1455-2021>.

- Trouet, V., Van Oldenborgh, G.J., 2013. KNMI climate explorer: A web-based research tool for high-resolution paleoclimatology. *Tree-Ring Res.* 69, 3–13. <https://doi.org/10.3959/1536-1098-69.1.3>.
- Wagner, S., Zorita, E., 2005. The influence of volcanic, solar and CO<sub>2</sub> forcing on the temperatures in the Dalton Minimum (1790–1830): a model study. *Clim. Dyn.* 25, 205–218. <https://doi.org/10.1007/s00382-005-0029-0>.
- Wang, B., Wu, R.G., Fu, X.H., 2000. Pacific–East Asian teleconnection: How does ENSO affect East Asian climate? *J. Clim.* 13 (9), 1517–1536. [https://doi.org/10.1175/1520-0442\(2000\)013<1517:PEATHD>2.0.CO;2](https://doi.org/10.1175/1520-0442(2000)013<1517:PEATHD>2.0.CO;2).
- Wang, H.Q., Chen, F., Yuan, Y.J., Yu, S.L., Shang, H.M., Zhang, T.W., 2013. Temperature signals in tree-ring width chronologies of alpine treeline conifers from the Baishui River Nature Reserve, China. *Terr. Atmos. Ocean. Sci.* 24 (6), 887–898. [https://doi.org/10.3319/TAO.2013.06.18.01\(A\)](https://doi.org/10.3319/TAO.2013.06.18.01(A)).
- Wang, J.L., Yang, B., Qin, C., Kang, S.Y., He, M.H., Wang, Z.Y., 2014. Tree-ring inferred annual mean temperature variations on the southeastern Tibetan Plateau during the last millennium and their relationships with the Atlantic Multidecadal Oscillation. *Clim. Dyn.* 43 (3), 627–640. <https://doi.org/10.1007/s00382-013-1802-0>.
- Wang, J.L., Yang, B., Ljungqvist, F.C., 2015. A millennial summer temperature reconstruction for the eastern Tibetan Plateau from tree ring width. *J. Clim.* 28 (13), 5289–5304. <https://doi.org/10.1175/JCLI-D-14-00738.1>.
- Way, D.A., Oren, R., 2010. Differential responses to changes in growth temperature between trees from different functional groups and biomes: a review and synthesis of data. *Tree Physiol.* 30, 669–688. <https://doi.org/10.1093/treephys/tpq015>.
- Wigley, T.M.L., Briffa, K.R., Jones, P.D., 1984. On the Average Value of Correlated Time Series, with Applications in Dendroclimatology and Hydrometeorology. *J. Appl. Meteorol. Climatol.* 23 (2), 201–213. [https://doi.org/10.1175/1520-0450\(1984\)023<201:OTAVOC>2.0.CO;2](https://doi.org/10.1175/1520-0450(1984)023<201:OTAVOC>2.0.CO;2).
- Wu, X., Li, J.J., Cui, L.L., Wu, X.F., Yang, K.Q., de Jesus, A.L., 2025. A 219-year tree-ring evidence revealing the influence of the Atlantic Multi-decadal Oscillation on annual mean temperature in the northern Western Sichuan Plateau. *Clim. Dyn.* 63, 135. <https://doi.org/10.1007/s00382-025-07629-4>.
- Xiao, D.M., Qin, N.S., Huang, X.M., 2015. A 325-year reconstruction of July–August mean temperature in the north of West Sichuan derived from tree-ring (in Chinese with English abstract). *Quat. Sci.* 35 (5), 1134–1144. <https://doi.org/10.11928/j.issn.1001-7410.2015.05.09>.
- Xiao, D.M., Huang, X.M., Qin, N.S., 2018. Tree-ring based annual precipitation reconstruction for the southern Three-River Headwaters region, China. *J. Water Clim. Chang.* 9 (3), 611–623. <https://doi.org/10.2166/wcc.2018.190>.
- Xu, P., Zhu, H.F., Shao, X.M., Yin, Z.Y., 2012. Tree ring-dated fluctuation history of Midui glacier since the Little Ice Age in the southeastern Tibetan Plateau. *Sci. China Earth Sci.* 55, 521–529. <https://doi.org/10.1007/s11430-011-4338-3>.
- Xu, S.S., Zheng, C.G., Shang, Z.Y., Zhang, Z.G., Kong, X.G., Robertson, I., Zhao, Z.J., 2024. A 903-year annual temperature reconstruction for the southeastern Tibetan Plateau from the tree ring widths of Juniperus saltuaria. *Sci. Rep.* 14, 27623. <https://doi.org/10.1038/s41598-024-79096-6>.
- Yang, B., Kang, X., Bräuning, A., Liu, J., Qin, C., Liu, J.J., 2010. A 622-year regional temperature history of Southeast Tibet derived from tree rings. *Holocene* 20, 181–190. <https://doi.org/10.1177/0959683609350388>.
- Yang, B., Qin, C., Bräuning, A., Osborn, T.J., Trouet, V., Charpentier Ljungqvist, F., Esper, J., Schneider, L., Grießinger, J., Büntgen, U., Rossi, S., Dong, G.H., Yan, M., Ning, L., Wang, J.L., Wang, X.F., Wang, S.M., Luterbacher, J., Cook, E.R., Stenseth, N.C., 2021. Long-term decrease in Asian monsoon rainfall and abrupt climate change events over the past 6,700 years. *Proc. Natl. Acad. Sci. USA* 118 (30), e2102007118. <https://doi.org/10.1073/pnas.2102007118>.
- Yao, T.D., Jiao, K.Q., Tian, L.D., Yang, Z.H., Shi, W.L., 1996. Climatic variations since the Little Ice Age recorded in the Guliya Ice Core. *Sci. China Ser. D Earth Sci.* 39 (6), 587–596. <https://www.sciengine.com/doi/10.1360/yd1996-39-6-587>.
- Yin, H., Liu, H.B., Linderholm, H.W., Sun, Y., 2015. Tree ring density-based warm-season temperature reconstruction since A.D. 1610 in the eastern Tibetan Plateau. *Palaeogeogr. Palaeoclimatol. Palaeoecol.* 426, 112–120. <https://doi.org/10.1016/j.palaeo.2015.03.003>.
- Yin, H., Sun, Y., Li, M.Y., 2022. Reconstructed temperature change in late summer over the eastern Tibetan Plateau since 1867 CE and the role of anthropogenic forcing. *Glob. Planet. Chang.* 208, 103715. <https://doi.org/10.1016/j.gloplacha.2021.103715>.
- You, Q.L., Min, J.Z., Kang, S.C., 2015. Rapid warming in the Tibetan Plateau from observations and CMIP5 models in recent decades. *J. Clim.* 38, 2896–2911. <https://doi.org/10.1002/joc.4520>.
- Yu, S.L., Yuan, Y.J., Wei, W.S., Zhang, T.W., Cheng, F., 2012. Reconstructed mean temperature in Mearkang, West Sichuan in July and its detection of climatic period signal. *Plateau Meteorol.* 31 (1), 193–200 (in Chinese).
- Yuan, Y.Y., Deng, Y., Gao, L.L., Fu, X.Y., Xu, Y.J., Gou, X.H., 2024. Unprecedented recent warming as recorded by tree-ring in the western Qinling Mountains, China. *Palaeogeogr. Palaeoclimatol. Palaeoecol.* 644, 112202. <https://doi.org/10.1016/j.palaeo.2024.112202>.
- Zhang, Q.B., Cheng, G.D., Yao, T.D., Kang, X.C., Huang, J.G., 2003. A 2,326-year tree-ring record of climate variability on the northeastern Qinghai-Tibetan Plateau. *Geophys. Res. Lett.* 30 (14), 1739. <https://doi.org/10.1029/2003GL017425>.
- Zhang, R., Sumi, A., Kimoto, M., 1996. Impact of El Niño on the East Asian monsoon: A diagnostic study of the '86/'87 and '91/'92 events. *J. Meteorol. Soc. Jpn.* 74, 49–62. <https://doi.org/10.2151/jmsj1965.74.1.49>.
- Zhang, Y., Li, J.J., Zheng, Z.Y., Zeng, S.L., 2021. A 479-year early summer temperature reconstruction based on tree-ring in the southeastern Tibetan Plateau China. *Atmosphere* 12 (10), 1251. <https://doi.org/10.3390/atmos12101251>.
- Zhang, Y., Li, J.J., Wang, S., Shao, X.M., Qin, N.S., An, W.L., 2022. A reconstruction of June–July temperature since AD 1383 for Western Sichuan Plateau, China using tree-ring width. *Int. J. Climatol.* 42 (3), 1803–1817. <https://doi.org/10.1002/joc.7336>.
- Zhou, P.F., Tang, J.P., Ma, M.N., Ji, D.B., Shi, J.C., 2024. High resolution Tibetan Plateau regional reanalysis 1961–present. *Sci Data* 11, 444. <https://doi.org/10.1038/s41597-024-03282-4>.
- Zhu, H.F., Shao, X.M., Yin, Z.Y., Huang, L., 2011. Early summer temperature reconstruction in the eastern Tibetan plateau since ad 1440 using tree-ring width of *Sabina tibetica*. *Theor. Appl. Climatol.* 106, 45–53. <https://doi.org/10.1007/s00704-011-0419-7>.
- Zhu, L.J., Zhang, Y.D., Li, Z.S., Guo, B.D., Wang, X.C., 2016. A 368-year maximum temperature reconstruction based on tree-ring data in the northwestern Sichuan Plateau (NWSP), China. *Clim. Past* 12, 1485–1498. <https://doi.org/10.5194/cp-12-1485-2016>.
- Zhuo, Z.D., Hu, S.X., Zhang, X.G., Zhao, Z., Wang, Y.S., Liu, G.Y., 1978. Tree rings of the Kilienshan Region, and changes of the climate during the recent Thousand Years in China (in Chinese with English abstract). *J. Lanzhou Univ.* 2, 145–157. <https://doi.org/10.13885/j.issn.0455-2059.1978.02.013>.